Numerical simulation on structural behavior of UHPFRC beams with steel and GFRP bars

Doo-Yeol Yoo[a] and Nemkumar Banthia[*]

Department of Civil Engineering, The University of British Columbia,
6250 Applied Science Lane, Vancouver, BC V6T 1Z4, Canada

Abstract. This study simulates the flexural behavior of ultra-high-performance fiber-reinforced concrete (UHPFRC) beams reinforced with steel and glass fiber-reinforced polymer (GFRP) rebars. For this, micromechanics-based modeling was first carried out on the basis of single fiber pullout models considering inclination angle. Two different tension-softening curves (TSCs) with the assumptions of 2-dimensional (2-D) and 3-dimensional (3-D) random fiber orientations were obtained from the micromechanics-based modeling, and linear elastic compressive and tensile models before the occurrence of cracks were obtained from the mechanical tests and rule of mixture. Finite element analysis incorporating smeared crack model was used due to the multiple cracking behaviors of structural UHPFRC beams, and the characteristic length of two times the element width (or two times the average crack spacing at the peak load) was suggested as a result of parametric study. Analytical results showed that the assumption of 2-D random fiber orientation is appropriate to a non-reinforced UHPFRC beam, whereas the assumption of 3-D random fiber orientation is suitable for UHPFRC beams reinforced with steel and GFRP rebars due to disorder of fiber alignment from the internal reinforcements. The micromechanics-based finite element analysis also well predicted the serviceability deflections of UHPFRC beams with GFRP rebars and hybrid reinforcements.

Keywords: ultra-high-performance fiber-reinforced concrete; flexure; micromechanics; fiber orientation; reinforcement; finite element analysis

1. Introduction

Recently developed ultra-high-performance fiber-reinforced concrete (UHPFRC) exhibits excellent mechanical strength, toughness, and durability (Richard and Cheyrezy 1995). In particular, due to its unique strain-hardening characteristics with multiple micro-cracks, UHPFRC is mechanically more performant than the conventional strain-softening concretes and useful in structures dominated by bending (Naaman and Reinhardt 2003). However, the real application of

---

∗Corresponding author. Professor, E-mail: banthia@civil.ubc.ca
[a] Postdoctoral Fellow, Ph.D., E-mail: dyyoo2@gmail.com

UHPFRC to civil infrastructures has been limited until today due to several demerits such as high cost, high deviation of tensile performance in terms of fiber orientation, and insufficient structural design and analysis technique. In order to overcome these drawbacks, many researchers (Wille *et al.* 2011, Kang *et al.* 2011, Yang *et al.* 2011, Ferrara 2012, Yoo 2014, Yoo *et al.* 2014a) have been performed material and structural tests of UHPFRC. Wille *et al.* (2011) and Yoo *et al.* (2014a) reported that the tensile and flexural performances of common UHPFRC including short smooth steel fibers can be improved by using twisted steel fibers and long smooth steel fibers, and thus, the fiber contents required for a certain level of tensile or flexural performance can be reduced. In general, 2% by volume of steel fibers occupies approximately 33% of total cost of UHPFRC (Yoo and Yoon 2015). Kang *et al.* (2011) and Ferrara (2012) noted that the flexural performance of UHPFRC is strongly influenced by the fiber orientation, and proper casting process leads to adequate fiber enhancement, better flexural performance, and high precision of test results. In addition, Yang *et al.* (2011) and Yoo (2014) performed structural tests of UHPFRC beams with non-prestressed and prestressed reinforcing steel and predicted their flexural behaviors according to two international recommendations (AFGC/SETRA 2002, JSCE 2004). Since the unique tensile properties of UHPFRC were considered in the analysis using tension-softening curve (TSC) obtained from fracture mechanics-based inverse analysis, the predicted values showed good agreement with the test data. However, to obtain adequate TSC of UHPFRC, three-point bending tests for small beams and complicated inverse analysis have been imperatively required.

Accordingly, to provide more simplified analytical technology, a micromechanics-based modeling for post-cracking TSC of UHPFRC was introduced in this study. Based on single fiber pullout models considering inclination angle, fiber bridging curves were first calculated with the assumptions of 2-dimensional (2-D) and 3-dimensional (3-D) random fiber orientations. Since the TSC consists of matrix softening and fiber bridging curves, a bilinear matrix softening curve, previously suggested by Yoo (2014), was adopted, and linear elastic compressive and pre-cracking tensile models obtained from experiments and rule of mixture were applied. Subsequently, finite element analyses incorporating the suggested material models were performed to simulate flexural behaviors of structural UHPFRC beams with steel and glass fiber-reinforced polymer (GFRP) rebars and verified through comparison with the previous test results by Yoo (2014).

2. Material models for UHPFRC and reinforcements

2.1 Pullout modeling of single fiber according to inclination angle

In order to obtain TSC, fiber pullout load and slip relation was first derived. Naaman *et al.* (1991) suggested basic mathematical equations for simulating the pullout response of smooth steel fiber. However, since these equations have been derived from the test results of smooth steel fiber embedded in normal- or high-strength cementitious matrix, the prediction of descending branch in full debonding region was inappropriate to the smooth steel fiber embedded in ultra-high-strength cementitious matrix. For this reason, Lee *et al.* (2010) proposed a modified model for predicting the pullout response of the smooth steel fiber embedded in ultra-high-strength cementitious matrix.

The pullout load and slip models considering snubbing and matrix spalling effects are as follows. The detailed procedure obtaining the following equations can be found elsewhere (Yoo *et al.* 2015c).

• Perfect bonding region in ascending branch:

$$\left(\frac{P}{\delta}\right)(\theta) = \frac{1/2}{1+\gamma\left(\frac{2\theta}{\pi}\right)^n}\frac{\lambda A_m E_m}{Q-2}\frac{1+e^{-\lambda l}}{1-e^{-\lambda l}} \tag{1}$$

where

$$\lambda = \sqrt{KQ} \tag{2}$$

$$K = \frac{\pi d_f \kappa}{A_m E_m} \tag{3}$$

$$Q = 1 + \frac{A_m E_m}{A_f E_f} \tag{4}$$

where P is the pullout load, δ is the slip displacement, θ is the inclination angle of fiber with respect to the loading direction, γ and n are the coefficients for considering the increase of slip capacity with the inclination angle ($\gamma = 100$ and $n = 2$ by Lee *et al.* (2010)), A_m and E_m are the area and elastic modulus of matrix, l is the embedment length of fiber, d_f is the diameter of fiber, κ is the initial slope of bond stress-slip relation, and A_f and E_f are the area and elastic modulus of fiber.

  • Partial debonding region in ascending branch:

$$P(\theta) = \pi d_f \tau_{f(\text{app})}(\theta)u + \frac{\pi d_f \tau_{\max(\text{app})}(\theta)}{\lambda}\frac{1-e^{-2\lambda(l-u)}}{\frac{2}{Q}e^{-\lambda(l-u)} + \left(1-\frac{1}{Q}\right)\left[1+e^{-2\lambda(l-u)}\right]} \tag{5}$$

$$\delta(\theta) = \left[1+\gamma\left(\frac{2\theta}{\pi}\right)^n\right]\frac{2}{A_m E_m}\left\{P(\theta)(Q-1)u - \frac{\pi d_f \tau_{f(\text{app})}(\theta)u^2}{2}(Q-2)\right.$$
$$\left. + \left(P(\theta) - \pi d_f \tau_{f(\text{app})}(\theta)u\right)\left[\frac{1-e^{-\lambda(l-u)}}{1+e^{-\lambda(l-u)}}\right]\frac{Q-2}{\lambda} - \pi d_f \tau_{f(\text{app})}(\theta)ul\right\} \tag{6}$$

where $\tau_{f(\text{app})}$ is the apparent frictional shear strength, $\tau_{\max(\text{app})}$ is the apparent bond strength, and u is the length of debonding zone.

Table 1 Physical and geometrical properties of matrix and steel fiber

Matrix			Steel fiber					
A_m (mm^2)	E_m (MPa)	v_m	d_f (mm)	l_f (mm)	A_f (mm^2)	f_t (MPa)	E_f (MPa)	v_f
3.14	45000	0.2	0.2	13.0	0.0314	2500	200000	0.3

Where, A_m = area of matrix ($100 \times A_f$), E_m = elastic modulus of matrix, v_m = Poisson's ratio of matrix, d_f = diameter of fiber, l_f = length of fiber ($2 \times$ embedment length of fiber), A_f = area of fiber, f_t = tensile strength of fiber, E_f = elastic modulus of fiber, and v_f = Poisson's ratio of fiber.

- Full debonding region in descending branch:

$$x = \left(l^2 - \delta l\right) / \left(l - 2\delta_0\right) \tag{7}$$

$$P = \pi d_f \tau_{fd}(\delta) x \tag{8}$$

$$\tau_{fd}(\delta) = \tau_{f(\text{app})}(\theta) \exp\left[-\eta(\delta - 2\delta_0)^\alpha\right] \frac{\left(1 - \exp\left\{\dfrac{-2v_f \mu x}{E_f r_f \left[\dfrac{(1+v_m)}{E_m} + \dfrac{(1-v_f)}{E_f}\right]}\right\}\right)}{\left(1 - \exp\left\{\dfrac{-2v_f \mu l}{E_f r_f \left[\dfrac{(1+v_m)}{E_m} + \dfrac{(1-v_f)}{E_f}\right]}\right\}\right)} \tag{9}$$

where δ_0 is the end slip of fiber at the onset of full debonding, τ_{fd} is the decaying frictional shear stress, η is the factor reflecting steepness of descending branch in fiber pullout curve, α is the coefficient determining initial slope of frictional slip behavior, v_f is the Poisson's ratio of fiber, μ is the frictional coefficient at the fiber-matrix interface, and v_m is the Poisson's ratio of matrix. The parameters η and α were assumed to be 0.05 and 1, respectively, according to a previous study (Lee *et al*. 2010). In addition, the properties of matrix and steel fiber are summarized in Table 1.

Based on the pullout test results performed by Yoo *et al*. (2013), the bond strength was found to be 7.55 MPa for the smooth steel fiber (l_f/d_f = 13/0.2 mm/mm, where l_f is the fiber length) embedded in ultra-high-strength matrix. The material properties and mix proportion for the structural UHPFRC beams simulated in this study were exactly same with those in a previous study (Yoo *et al*. 2013). Therefore, the bond strength of 7.55 MPa was adopted.
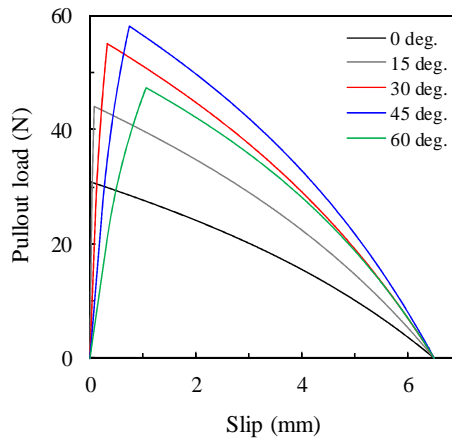

Fig. 1 Analytical pullout load and slip curves of smooth steel fiber embedded in ultra-high-strength matrix according to inclination angle (bond strength of 7.55 MPa)

Table 2 Material properties of UHPFRC

τ_{max} (MPa)	f_c' (MPa)	E_c (MPa)	ε_c' (mm/mm)	f_{ti}^* (MPa)
7.55	196.7	47800	4.4×10^{-3}	10.95

Where, τ_{max} = bond strength, f_c' = compressive strength, E_c = elastic modulus, ε_c' = compressive strain at the peak, and f_{ti} = first cracking tensile strength
* f_{ti} is calculated by rule of mixture.

The calculated pullout load versus slip responses of single smooth steel fiber with various inclination angles are shown in Fig. 1. The variations of the maximum pullout load and the corresponding slip were well simulated using Eqs. (1)–(9); the pullout load increased up to the inclination angle of 45°, while the slip continuously increased with the inclination angle.

2.2 Micromechanics-based material modeling for UHPFRC

Linear elastic compressive and tensile models before the occurrence of cracks were adopted, and the properties used are summarized in Table 2. Compressive strength and elastic modulus obtained from experiments were found to be 196.7 MPa and 47.8 GPa, respectively, and the first cracking tensile strength was calculated based on rule of mixture and found to be 10.95 MPa.

For the modeling of post-cracking tensile behavior, the TSC composed of matrix softening curve and fiber bridging curve is required. The fiber bridging curve can be calculated by extending the pullout model of single fiber to multiple fibers with consideration of fiber orientation. Not only was the evaluation of actual fiber orientation characteristics in large UHPFRC beams with reinforcements difficult, but also the flexural behavior of small UHPFRC beams was quite well predicted by assuming the 2-D random fiber orientation in a previous study (Yoo *et al*. 2015c). Thus, the fiber orientation was simply assumed to be 2-D and 3-D random in this study. The probability density functions (PDFs) for 2-D and 3-D random fiber orientations were used by $2/\pi$ and $\sin\theta$, respectively.

The number of fibers per unit area is influenced by the fiber orientation and the embedded length, as expressed by

$$N_b = N_{1D} \int_0^{\pi/2} \int_0^{l_f/2} p(l)p(\theta)\cos\theta \, dl \, d\theta \tag{10}$$

where N_{1D} is the number of fibers per unit area for 1-D ($N_{1D} = V_f/A_f$), V_f is the volume fraction of steel fiber, and $p(l)$ and $p(\theta)$ are the PDFs for embedment length and inclination angle.

The resistance force of a single fiber at the crack plane is given by a function of inclination angle θ, embedded length l, and amount of slip δ. Thus, the bridging stress of the composites σ_b is expressed by

$$\sigma_b(\delta) = \frac{4V_f}{\pi d_f^2} \int_0^{\pi/2} \int_0^{l_f/2} P(\theta, l, \delta)p(l)p(\theta)\cos\theta \, dl \, d\theta \tag{11}$$

For the case of matrix softening, the following equations suggested by Yoo (2014) were adopted.

$$\sigma_{mt} = f_t \left[1 - (1-a)\frac{w}{w_1} \right] \text{ for } af_t \leq \sigma_{mt} \leq f_t \tag{12}$$

$$\sigma_{mt} = \frac{af_t}{w_c - w_1}(w_c - w) \text{ for } 0 \leq \sigma_{mt} \leq af_t \tag{13}$$

where f_t is the first cracking tensile strength in composites ($= f_{ti}$) and the parameters in the bilinear matrix softening curve a, w_1, and w_c were used by 0.3, 0.15, and 0.7, respectively.

Fig. 2 shows the calculated fiber bridging curves and matrix softening curve. Higher maximum fiber bridging stress of 8.99 MPa was obtained for the 2-D random fiber orientation than that of 3-D random fiber orientation. This is because better fiber orientation for the case of 2-D random fiber orientation led to higher number of fibers at the crack surfaces than its counterpart, as reported by Yoo *et al*. (2015b).
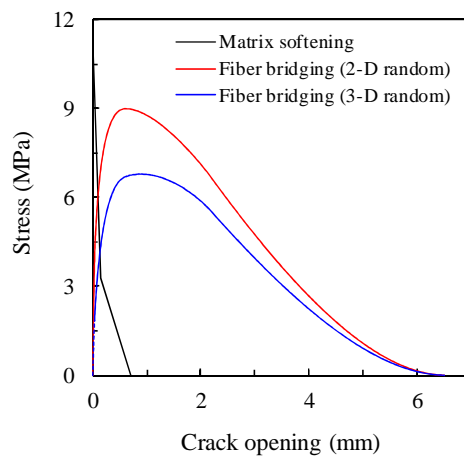

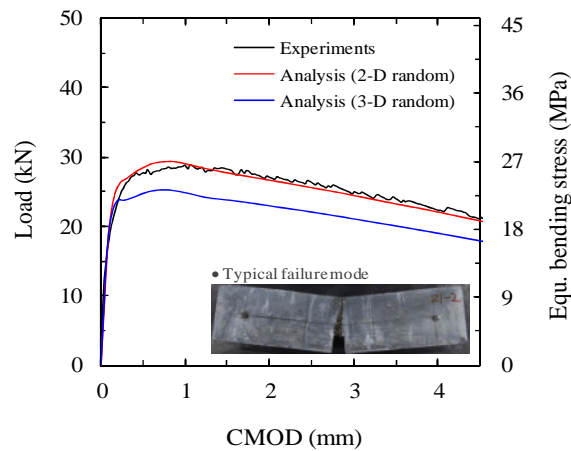Fig. 2 Matrix softening and fiber bridging curves

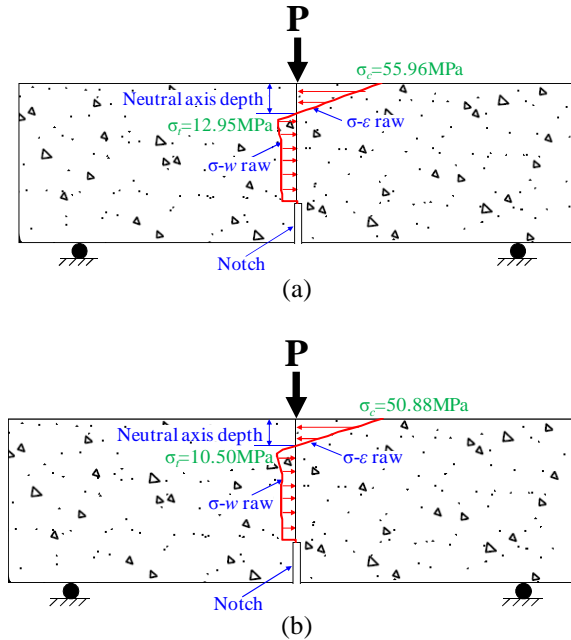Fig. 3 Comparison of experimental and analytical results (small UHPFRC beams)

Fig. 4 Stress distribution along the beam height at the peak load; (a) 2-D random orientation (P_{peak} = 29.3 kN and c =18.0 mm), (b) 3-D random orientation (P_{peak} = 23.2 kN and c = 15.8 mm) (Note: P_{peak} is the peak load and c is the neutral axis depth)

To verify the modeled TSC, flexural response of small UHPFRC beams ($100 \times 100 \times 400$ mm) with 30 mm notch at the mid-length was predicted through the sectional analysis. Fig. 3 shows the comparison of load versus crack mouth opening displacement (CMOD) curves obtained from the experiments and the micromechanics-based sectional analyses. The analytical result using the fiber bridging curve based on the PDF assuming 2-D random fiber orientation showed fairly good agreement with the test data. The peak load, CMOD at the peak, and post-peak softening behavior were well predicted. In contrast, the prediction using the fiber bridging curve based on the PDF assuming 3-D random fiber orientation exhibited lower load carrying capacity than the test data. This indicates that the assumption of 2-D random fiber orientation is appropriate to be used for predicting the flexural response of small UHPFRC beams rather than the assumption of 3-D random fiber orientation.

Fig. 4 exhibits the stress distribution along the beam height at the peak load. Regardless of the fiber orientation, the compressive stress at the top fiber was much lower than the compressive strength (f_c'= 196.7 MPa). On the other hand, the flexural crack was quite deeply propagated into the compressive zone at the peak load. This means that the beam was dominantly failed by the flexural crack rather than the concrete crushing, as shown in Fig. 3 (for typical failure mode of notched UHPFRC beam). The stress distribution was influenced by the fiber orientation; 2-D random fiber orientation provided higher maximum compressive and tensile stresses and neutral axis depth than those of the 3-D random fiber orientation. This is because a higher fiber bridging stress at the peak load obtained in the 2-D random fiber orientation leads to higher compressive and tensile stresses and neutral axis depth (by force equilibrium condition at the cross-section), compared to that in the 3-D random fiber orientation.

3. Numerical analysis and verifications

3.1 Steel bar-reinforced UHPFRC beams under four-point bending load

3.1.1 Analytical procedure

There are two analytical models, i.e., (1) smeared crack model and (2) discrete crack model, mainly used for predicting the flexural response of fiber-reinforced concrete (FRC). These models can take into account the unique tensile behaviors by incorporating TSCs. However, since the steel bar-reinforced UHPFRC beams produced numerous micro-cracks and showed various failure modes, the smeared crack model is more appropriate than the discrete crack model. This is because the discrete crack approach needs pre-defined crack path, whereas the smeared crack approach dose not require the pre-defined cracks and the crack opening is assumed to be smeared out over a characteristic length. Thus, the smeared crack model was adopted in this study.

The smeared crack approach provides different predictions according to the characteristic length (= crack band width). In the case of normal-strength concrete, the characteristic length is appropriate to be defined by the width of element or square root of element area. However, Denarié *et al*. (2003) reported that in contrast to normal-strength concrete, different characteristic lengths are required in some special cases (i.e., FRC, high-performance fiber-reinforced cementitious composites (HPFRCC), UHPFRC, etc.). In addition, if inappropriate characteristic length is assumed, the predicted crack pattern will be unrealistic and the ductility and load carrying capacity will be overestimated or underestimated. For this, the preliminary studies for determining an adequate characteristic length are imperative.

Fig. 5 shows the geometry and finite element meshes for steel bar-reinforced UHPFRC beam. The commercial program DIANA (TNO 2002) was used. Because of its symmetry, a half model of
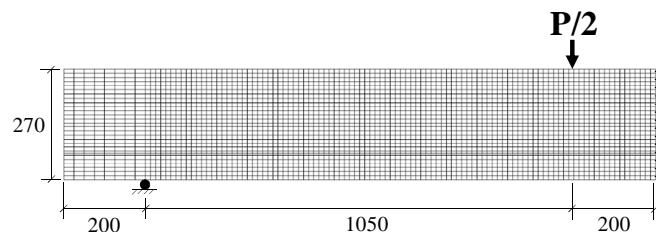

Fig. 5 Finite element meshes for steel bar-reinforced UHPFRC beam under four-point bending load (unit: mm)
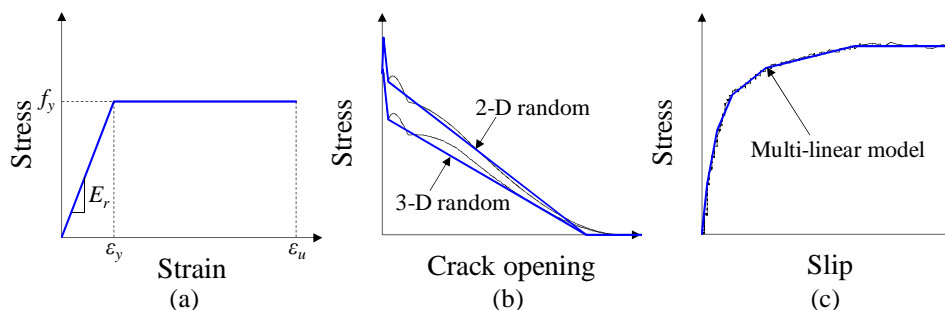

Fig. 6 Models for FE analysis; (a) stress-strain model of steel rebar, (b) TSCs for UHPFRC, (c) bond stress-slip model

the beam was adopted to save computing time. To model the concrete, a four-node quadrilateral isoparametric plane stress element (Q8MEM) based on linear interpolation and Gauss integration was used. In addition, a bilinear material model for the steel rebar with a nominal diameter of 12.7 mm, yield strength of 522.7 MPa, elastic modulus of 200.0 GPa, and ultimate strain of 0.164 mm/mm was adopted, as shown in Fig. 6(a). The total number of elements and number of nodes used were 2916 and 3052, respectively. The modeled element width in clear span length was adopted by 12.5 mm, similar to the experimentally obtained average crack spacing at the peak load (Yoo 2014). The smeared crack approach in DIANA requires only up to 5 points in the TSC. Therefore, the TSCs obtained from micromechanics-based analysis were simplified as shown in Fig. 6(b).

In order to consider bond stress-slip response between steel rebar and concrete, multi-linear bond-slip model was adopted based on the pullout test results performed by Yoo *et al*. (2014b), as shown in Fig. 6(c). Due to the extremely high bond strength of UHPFRC, steel yielding is generally obtained when an embedment length is higher than two times the rebar diameter. For this reason, only ascending part in the bond-slip response was modeled in this study. The bond stress-slip model is composed of normal and shear tractions versus slip relationships. The normal traction-slip response was assumed to be linear elastic, while the shear traction-slip response was adopted from the multi-linear model in Fig. 6(c).

3.1.2 Preliminary analysis for determination of characteristic length

The numerical analysis results, based on smeared crack model, are influenced by the characteristic length. In order to determine an adequate characteristic length l_c, the flexural response of UHPFRC beam without reinforcement was predicted with the assumption of 2-D random fiber orientation and with three different characteristic lengths ($l_c = 1 \times b_e$, $2 \times b_e$, and $3 \times b_e$, where b_e is the element width). The reason why 2-D random fiber orientation was assumed is because; (1) to obtain real fiber orientation for structural UHPFRC beam was difficult and (2) based on the previous analytical results by Yoo *et al*. (2015c), UHPFRC beam without reinforcement was fairly well predicted by assuming 2-D random fiber orientation.

Fig. 7 shows the comparison of experimental and analytical results for the peak load and the corresponding deflection. The peak load and the corresponding deflection were strongly affected
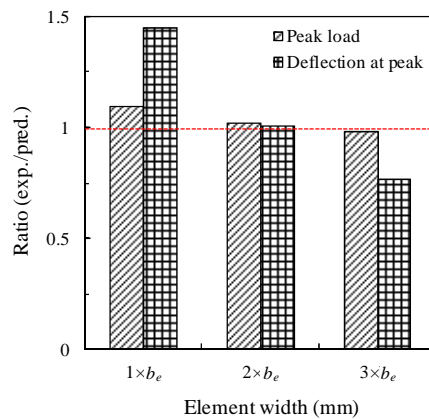

Fig. 7 Effect of characteristic length on the ratios of peak loads and deflections at the peak obtained from experiments and predictions

by the characteristic length; these values decreased with an increase in the characteristic length. For the case of $l_c = 2 \times b_e$ ($l_c = 25$ mm), the analytical prediction exhibited good agreement with the test data. Therefore, the characteristic length of two times the element width ($2 \times b_e$) (or two times the average crack spacing at the peak load) was adopted.

3.1.3 Comparison of experimental and numerical results

In Fig. 8, the comparison is made between the experimental and the analytical results. To evaluate the suitability of the suggested micromechanics-based material models and smeared crack approach, sectional analysis, which incorporates TSC obtained from inverse analysis, was also performed on the basis of AFGC/SETRA recommendations (AFGC/SETRA 2002, Yoo 2014). The moment-curvature relations obtained from the sectional analyses were converted to the load-deflection relations in terms of the linear elastic theory, as expressed by

$$F = \frac{4M}{\left(L - L_p\right)} \tag{14}$$

$$\Delta = \phi \frac{3L^2 - 4L_1^2}{24} \tag{15}$$

where F is the applied load, M is the moment, L is the span length, L_p is the length of pure moment region, Δ is the deflection, ϕ is the curvature, and $L_1 = (L - L_p)/2$.

In the case of UHPFRC beam without reinforcement, the micromechanics-based finite element (FE) analysis with the assumption of 2-D random fiber orientation provided the best prediction to the present test data, whereas the micromechanics-based FE analysis with the assumption of 3-D random fiber orientation showed a lower load carrying capacity than the test data. Therefore, it was noted that the FE analysis with the assumption of 2-D random fiber orientation is appropriate to predict the flexural responses of UHPFRC beams without reinforcement. On the other hand, the sectional analysis showed slightly lower peak load and larger deflection at the peak than the experimental results.

For the UHPFRC beams with steel rebars, the FE analyses and sectional analyses exhibited slightly stiffer pre-peak load-deflection curves than the experiments. The predictions based on the FE analysis with the assumption of 2-D random fiber orientation showed higher load carrying capacities than the test data. On the contrary, the FE analysis with the assumption of 3-D random fiber orientation exhibited fairly good agreement with the test data, especially for the beams including four and six steel rebars ($\rho = 1.06\%$ and $\rho = 1.71\%$). This is attributed to the fact that the fiber alignment along the flow direction was disturbed by the internal steel rebars. Therefore, it was concluded that the assumption of 3-D random fiber orientation is more appropriate to predict the flexural response of UHPFRC beams with steel rebars than that of 2-D random fiber orientation. The sectional analyses showed median values between the 2-D and 3-D random fiber orientations and quite well predicted the peak loads and the corresponding deflections. As shown in Fig. 8(b), which is the typical principle strain and stress contour and the deformed shape of the beam at the ultimate, the compressive and tensile strains and stresses were well distributed along the height of beam. The highest tensile and compressive stresses and strains for both the concrete and steel rebar were obtained in the pure maximum moment region.

3.2 GFRP bar- and hybrid-reinforced UHPFRC beams under three-point bending load

3.2.1 Analytical procedure

In order to predict the flexural response of UHPFRC beams reinforced with GFRP rebars and hybrid reinforcements, micromechanics-based FE analysis was also conducted. Since the assumption of 3-D random fiber orientation provided better prediction than that of 2-D random fiber orientation for the UHPFRC beams including steel rebars, 3-D random fiber orientation was only considered for modeling the UHPFRC beams with GFRP rebars and hybrid reinforcements. A bilinear model was used for steel rebar in Fig. 6(a), and a linear elastic model for GFRP rebar with ultimate strength of 1182.0 MPa and elastic modulus of 51.3 GPa was applied, as shown in Fig. 9(a). The detailed properties of used steel and GFRP rebars are summarized in Table 3.

To take into account the bond stress and slip relationships, multi-linear bond stress-slip models were used. For steel rebar, the bond stress-slip model in Fig. 6(c) was considered, while for GFRP
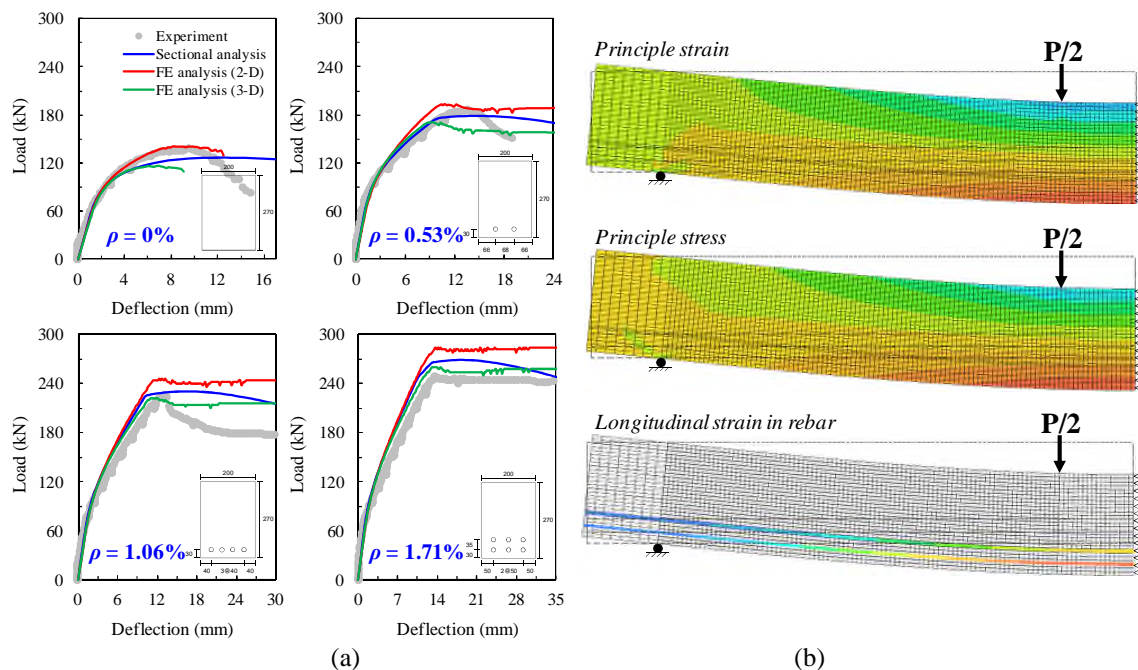

Fig. 8 Analytical results for steel bar-reinforced UHPFRC beams; (a) load-deflection curves, (b) contour of stresses and strains for UHPFRC beam with six steel rebars

Table 3 Mechanical and geometrical properties of steel and GFRP rebars

Type	d_r (mm)	A_r (mm^2)	E_r (MPa)	f_y (MPa)	ε_y (mm/mm)	f_u (MPa)	ε_u (mm/mm)
Steel rebar	12.7	126.7	200000	522.7	0.0026	-[*]	0.164
GFRP rebar	12.7	126.7	51300	-	-	1182.0	0.023

Where, d_r = nominal diameter of rebar, A_r = area of rebar, E_r = elastic modulus of rebar, f_y = yield strength of steel rebar, ε_y = yield strain of steel rebar, f_u = ultimate strength of GFRP rebar, and ε_u = ultimate strain of rebar

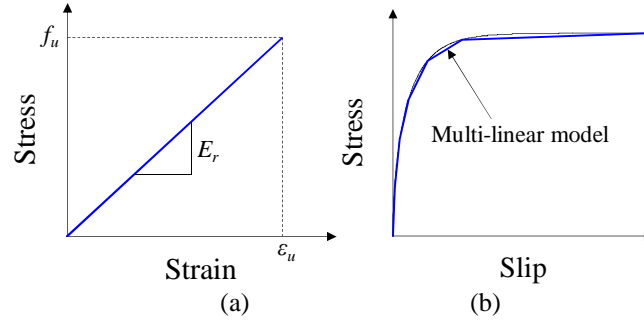[*] f_u is assumed to be identical with f_y for the case of steel rebar.

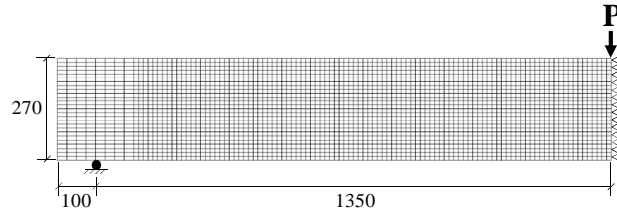Fig. 9 Models for FE analysis (GFRP rebar); (a) tensile stress-strain model, (b) bond stress-slip model

Fig. 10 Finite element meshes for UHPFRC beam with GFRP rebar and hybrid reinforcement under three-point bending load (unit: mm)

rebar, the multi-linear bond stress-slip model based on the following Eqs. (16) and (17) was used, as illustrated in Fig. 9(b). The bond stress-slip model for the GFRP rebar embedded in UHPFRC was obtained based on the previous pullout test results by Yoo *et al.* (2015a). The maximum bond strength of GFRP rebar was found to be 15.1 MPa from the following Eq. (16).

$$\frac{u}{\sqrt{f_c'}} = k_1 + k_2 \frac{d_r}{L_e} \tag{16}$$

where u is the bond strength of GFRP rebar, f_c' is the compressive strength, k_1 and k_2 are the curve fitting coefficients, d_r is the rebar diameter, and L_e is the embedment length of rebar. The coefficients k_1 and k_2 were obtained in terms of the curve fitting using the least-square error method and found to be 1.05 and 0.85, respectively (Yoo *et al.* 2015a).

In addition, the CMR model (Cosenza *et al.* 1995) was adopted for modeling the bond stress-slip response in the ascending branch, as expressed by

$$\tau = u\left(1 - e^{-s/s_r}\right)^{\beta} \tag{17}$$

where τ is the bond stress, s is the slip, and s_r and β are the curve fitting coefficients and obtained by $s_r = 0.16$ and $\beta = 0.50$, respectively (Yoo *et al.* 2015a).

In accordance with a previous model for development length of GFRP rebar in UHPFRC ($L_{d,pull-out} = d_r f_u / 3.4(f_c')^{0.5}$), the development length was obtained by approximately 310 mm. Therefore, pullout failure of GFRP rebars in UHPFRC beams was not observed, and only ascending part in the bondstress-slip curve was considered.

The geometry and finite element meshes for UHPFRC beams reinforced with GFRP rebars and hybrid reinforcements are shown in Fig. 10. In similar to the analysis used for steel bar-reinforced

UHPFRC beams, the Q8MEM was adopted for modeling UHPFRC, and a half model of the beam was used. Total number of elements and number of nodes were 3024 and 3161, respectively. The modeled element width in clear span length was 12.5 mm, similar to the measured average crack spacing at the peak load, and the smeared crack approach was adopted. Based on the previous parametric study, the characteristic length was also determined to be two times the element width.

3.2.2 Comparison of experimental and numerical results

Fig. 11 shows the comparison of the experimental and FE analytical results. The micromechanics -based FE analyses showed quite good agreement with the test data. In the case of UHPFRC beams reinforced with two GFRP rebars only or two inner steel and two outer GFRP rebars, the FE analysis showed slightly lower post-cracking load carrying capacity than the test data at the same deflection. This is attributed to the fact that the steel fibers were more aligned parallel to the flow direction than the 3-D random fiber orientation assumption because of the large spacing between rebars and form. On the other hand, for the beams including more GFRP rebars and hybrid reinforcements, the FE analyses generally exhibited similar (or slightly stiffer) post-cracking load-deflection response with the test data up to near the peak load. Because the elastic modulus of GFRP rebars is significantly lower than that of steel rebars, a higher deflection of GFRP bar-reinforced concrete beams is obtained in comparison with steel bar-reinforced beams having an identical reinforcement ratio (Nanni 1993). Therefore, it is important to accurately predict the serviceability deflection of GFRP bar-reinforced concrete beams.
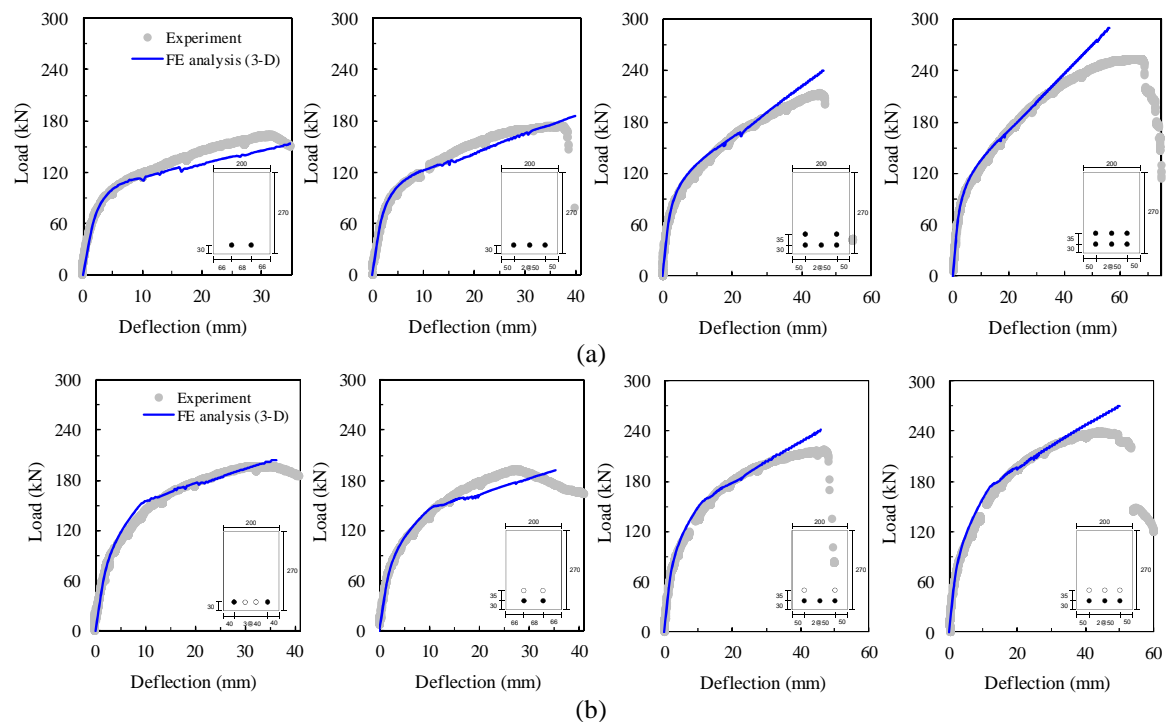

Fig. 11 Comparison of experimental and numerical results for UHPFRC beams with GFRP rebar and hybrid reinforcement; (a) GFRP bar-reinforced UHPFRC beams, (b) hybrid reinforced UHPFRC beams (black circle: GFRP rebar and white circle: steel rebar)
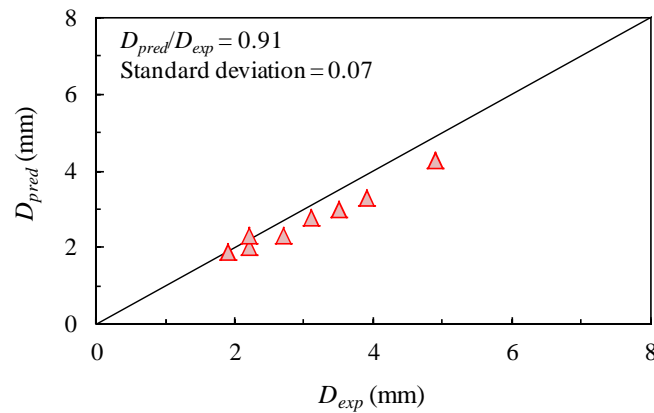
Fig. 12 Comparison of serviceability deflections, *D*, obtained from experiments and FE analysis

In accordance with a previous study by Yoo (2014), the previous models (ACI 2006, Bischoff 2005), which are most widely used for predicting the serviceability deflection, were inappropriate to predict serviceability deflection of UHPFRC beams with GFRP rebars and hybrid reinforcements due to its strain-hardening characteristics (i.e., the average ratios of serviceability deflections obtained from experiments and the previous models were found to be approximately 0.18). Thus, the micromechanics-based FE analysis was alternatively adopted to predict the serviceability deflection in this study. Fig. 12 shows the comparison of serviceability deflections, *D*, (at 40% of ultimate moment, M_u) (Issa *et al.* 2011) obtained from experiments and FE analyses with the assumption of 3-D random fiber orientation. Serviceability deflections were quite well predicted from the FE analysis; the average ratios of serviceability deflections from predictions and experiments, D_{pred}/D_{exp}, were found to be 0.91 (standard deviation of 0.07).

4. Conclusions

In this study, the flexural behavior of structural UHPFRC beams reinforced with steel and GFRP rebars was simulated by using micromechanics-based FE analysis. For the tensile modeling, two different fiber orientations (2-D and 3-D random) were considered, and smeared crack approach was adopted for FE analysis. Based on a parametric study, the characteristic length of two times the element width (or two times the average crack spacing at the peak load) was suggested for UHPFRC beams. The assumption of 2-D random fiber orientation showed the best prediction to the test results of UHPFRC beam without reinforcement. However, in the case of UHPFRC beams with steel and GFRP rebars, the assumption of 3-D random fiber orientation was more suitable than its counterpart (2-D random), because the fiber alignment was disturbed by the internal reinforcements. Lastly, the micromechanics-based FE analysis quite well predicted the serviceability deflections of UHPFRC beams reinforced with GFRP rebars and hybrid reinforcements.

Acknowledgements

References

American Concrete Institute (2006), Guide for the design and construction of concrete reinforced with FRP bars, ACI 440.1R-06, Farmington Hills, Michigan, IL.USA.

Association Francaise de Genie Civil (2002), "Ultra high performance fibre-reinforced concretes", AFGC/SETRA, Interim Recommendations, Bagneux, France.

Bischoff, P.H. (2005), "Reevaluation of deflection prediction for concrete beams reinforced with steel and fiber reinforced polymer bars", *J. Struct. Eng.*, **131**(5), 752-767.

Cosenza, E., Manfredi, G. and Realfonzo, R. (1995), "Analytical modelling of bond between FRP reinforcing bars and concrete", In: Taerwe L, editor. *Proceedings of second international RILEM symposium (FRPRCS-2)*. London: E and FN Spon.

Denarié, E., Habel, K. and Brühwiler, E. (2003), "Structural behavior of hybrid elements with advanced cementitious materials (HPFRCC)", *Fourth International Workshop on High Performance Fiber Reinforced Cement Composites (HPFRCC-4)*, RILEM, Ann Arbor, Michigan, IL.USA.

Ferrara, L. (2012), "High performance fiber reinforced self-compacting concrete (HPFRSCC): a "smart material" for high end engineering applications", *Proceedings of the 3rd International Workshop on Heterogeneous Architectures and Computing*, Madrid.

Issa, M.S., Metwally, I.M. and Elzeiny, S.M. (2011), "Influence of fibers on flexural behavior and ductility of concrete beams reinforced with GFRP rebars", *Eng. Struct.*, **33**(5), 1754-1763.

Japan Society of Civil Engineers (2004), "Recommendations for design and construction of ultra-high strength fiber reinforced concrete structures (Draft)", JSCE, Tokyo, Japan.

Kang, S.T., Lee, B.Y., Kim, J.K. and Kim, Y.Y. (2011), "The effect of fibre distribution characteristics on the flexural strength of steel fibre-reinforced ultra high strength concrete", *Const. Build. Mater.*, **25**(5), 2450-2457.

Lee, Y., Kang, S.T. and Kim, J.K. (2010), "Pullout behavior of inclined steel fiber in an ultra-high strength cementitious matrix", *Const. Build. Mater.*, **24**(10), 2030-2041.

Naaman, A.E. and Reinhardt, H.W. (2003), "High performance fiber reinforced cement composites HPFRCC 4: International RILEM Workshop", *Mater. Struct.*, **36**(10), 710-712.

Naaman, A.E., Namur, G.G., Alwan, J.M. and Najm, H.S. (1991), "Fiber pullout and bond slip. 1: analytical study", *J. Struct. Eng.*, **117**(9), 2769-2790.

Nanni, A. (1993), "Flexural behavior and design of RC members using FRP reinforcement", *J. Struct. Eng.*, **119**(11), 3344-3359.

Richard, P. and Cheyrezy, M. (1995), "Composition of reactive powder concretes" , *Cem. Concr. Res.*, **25**(7), 1501-1511.

TNO Building and Construction Research (2002), DIANA-8 user's manual, TNO DIANA BV, Delft, The Netherlands.

Wille, K., Kim, D.J. and Naaman, A.E. (2011), "Strain-hardening UHP-FRC with low fiber contents", *Mater. Struct.*, **44**(3), 583-598.

Yang, I.H., Joh, C. and Kim, B.S. (2011), "Flexural strength of large-scale ultra high performance concrete prestressed T-beams", *Can. J. Civil Eng.*, **38**(11), 1185-1195.

Yoo, D.Y. (2014), "Performance enhancement of ultra-high-performance fiber-reinforced concrete and model development for practical utilization", Ph.D. Thesis, Korea University, Seoul, Korea, 586 pp.

Yoo, D.Y. and Yoon, Y.S. (2015), "Structural performance of ultra-high-performance concrete beams with different steel fibers", *Eng. Struct.*, **102**, 409-423.

Yoo, D.Y., Kang, S.T., Lee, J.H. and Yoon, Y.S. (2013), "Effect of shrinkage reducing admixture on tensile and flexural behaviors of UHPFRC considering fiber distribution characteristics", *Cem. Concr. Res.*, **54**, 180-190.

Yoo, D.Y., Kang, S.T. and Yoon, Y.S. (2014a), "Effect of fiber length and placement method on flexural behavior, tension-softening curve, and fiber distribution characteristics of UHPFRC", *Const. Build. Mater.*, **64**, 67-81.

Yoo, D.Y., Shin, H.O., Yang, J.M. and Yoon, Y.S. (2014b), "Material and bond properties of ultra high performance fiber reinforced concrete with micro steel fibers", *Compos. Part B–Eng.*, **58**, 122-133.

Yoo, D.Y., Kwon, K.Y., Park, J.J. and Yoon, Y.S. (2015a), "Local bond-slip response of GFRP rebar in ultra-high-performance fiber-reinforced concrete", *Compos. Struct.*, **120**, 53-64.

Yoo, D.Y., Zi, G., Kang, S.T. and Yoon, Y.S. (2015b), "Biaxial flexural behavior of ultra-high-performance fiber-reinforced concrete with different fiber lengths and placement methods", *Cem. Concr. Compos.*, **63**, 51-66.

Yoo, D.Y., Kang, S.T., Banthia, N. and Yoon, Y.S. (2015c), "Nonlinear finite element analysis of ultra-high-performance fiber-reinforced concrete beams", *Int. J. Damage Mech.* DOI: 10.1177/1056789515612559

CC